Supplementary Information

Unravelling the formation pathway and energetic landscape of lanthanide cages based on bis-β-diketonato ligands

Maria Rando[a], Alice Carlotto[a], Silvia Carlotto[a,b], Roberta Seraglia[c], Marzio Rancan[b*] and Lidia Armelao[a,d]

[a] Department of Chemical Sciences, University of Padova, via F. Marzolo 1, 32131, Padova, Italy.

[b] Institute of Condensed Matter Chemistry and Technologies for Energy (ICMATE), National Research Council (CNR), c/o Department of Chemistry, University of Padova, via F. Marzolo 1, 35131 Padova, Italy.

[c] Institute of Condensed Matter Chemistry and Technologies for Energy (ICMATE), National Research Council (CNR), Corso Stati Uniti, 4, Padova PD, Italy.

[d] Department of Chemical Sciences and Materials Technologies (DSCTM), National Research Council (CNR), Piazzale A. Moro 7, 00185 Roma, Italy.

* e-mail: marzio.rancan@cnr.it

Index

1. Synthesis and characterization

Reagents were purchased from Aldrich and used as received.

^{1}H-NMR spectra were recorded with a Bruker 300 MHz spectrometer equipped with a BBO probe. DOSY analyses were performed with a Bruker 400 Avance III HD equipped with a BBI-z grad probehead.

Elemental analyses were performed with a ThermoScientific FLASH 2000 elemental analyser.

FT-IR spectra were recorded with a spectrometer Agilent Cary 630 equipped with an attenuated toral reflectance module in the 4000–650 cm^{-1} range and with a spectral resolution of 2 cm^{-1}.

Electrospray mass spectrometric measurements (ESI/MS) were performed using a LCQ Fleet ion trap instrument (ThermoFisher), equipped with a HESI source, operating in positive and negative ion modes. The mass spectra were acquired using the following experimental parameters: T_{HESI} = 35 °C; $T_{transfer\ capillary}$= 275 °C; Voltage $_{HESI}$= ± 4 kV; nebulizer gas flow rate (N_2): 10 a.u.; auxiliary gas flow rate (N_2): 5 a.u. Sample solutions (10^{-6} M in acetonitrile) were introduced by direct infusion using a syringe pump at a flow rate of 8 µl·min^{-1}.

1.1. Ligands synthesis

preL^A: synthesized by a previous methodology.[1] p-bromoacetophenone (3.58 g, 18.0 mmol), tert-butylcarbammate (0.70 g, 6.0 mmol), K_3PO_4 (7.64 g, 36.0 mmol), and CuI (0.35 g, 1.8 mmol), have been added in a Schlenk tube under argon atmosphere. Anhydrous toluene has been added as solvent (30 ml), together with N,N-dimethylethylenediamine (0.6 ml, 5.6 mmol). The mixture has been reacted at 110 °C for 45 h, under vigorous stirring. The reaction has been quenched by the addition of water (100 ml) and ethyl acetate (180 ml). The organic phase has been washed with water (3x100 ml), dried over $MgSO_4$ and the solvent has been removed under reduced pressure resulting in 3.44 g of a dark orange dense oil. The product has been purified by SiO_2 column chromatography (n-hexane/ethyl acetate 6:4) to give 2.06 g of a yellow solid. Yield: 97%.

preL^B: synthesized by a previous methodology.[2] In a 100 ml 3 necks round bottom flask, o-triphenylbenzene (2.35 g, 10.2 mmol) has been dissolved in 30 ml of anhydrous CH_2Cl_2 under argon atmosphere. $AlCl_3$ (3.50 g, 26.2 mmol) has been added to the solution, under vigorous stirring. After cooling the reaction mixture to 0 °C, a solution of acetyl chloride (1.85 ml, 26.0 mmol) in 5 ml of

anhydrous CH_2Cl_2 has been added. The mixture has been stirred at room temperature for 30 min, then it has been reacted at reflux for 3 h. After that, 100 g of ice and 25 ml of HCl 37% have been added. The mixture has been extracted with CH_2Cl_2 (3x40 ml). The organic phase has been washed with 5% $NaHCO_3$ aqueous solution (100 ml) and then with a saturated NaCl aqueous solution (40 ml). The organic phase has been dried over $MgSO_4$ and the solvent has been removed under reduced pressure resulting in 3.10 g of a yellow solid. The product has been purified by SiO_2 column chromatography (CH_2Cl_2) to give 1.94 g of white solid. Yield: 60%.

preL^M: synthesized by a previous methodology.[2] In a 100 ml 3 necks round bottom flask, diphenylmethane (1.69 g, 10.0 mmol) has been dissolved in 30 ml of anhydrous CH_2Cl_2 under argon atmosphere. $AlCl_3$ (3.40 g, 25.5 mmol) has been added to the solution, under vigorous stirring. After cooling the reaction mixture to 0 °C, a solution of acetyl chloride (1.85 ml, 26.0 mmol) in 5 ml of anhydrous CH_2Cl_2 has been added. The mixture has been stirred at room temperature for 30 min, then it has been reacted at reflux for 3 h. After that, 100 g of ice and 25 ml of HCl 37% have been added. The mixture has been extracted with CH_2Cl_2 (3x40 ml). The organic phase has been washed with 5% $NaHCO_3$ aqueous solution (100 ml) and then with a saturated NaCl aqueous solution (40 ml). The organic phase has been dried over $MgSO_4$ and the solvent has been removed under reduced pressure resulting in 2.51 g of a yellow solid. The product has been purified by SiO_2 column chromatography (n-hexane/ethyl acetate 6:4) to give 1.57 g of white solid. Yield: 62%.

L^A: synthesized by a previous methodology.[1] Metallic Na (0.67 g, 29.1 mmol) has been dissolved in absolute ethanol (40 ml), in a 100 ml 3 necks round bottom flask, under argon atmosphere. After the solution reached room temperature, ethyl trifluoroacetate (5.0 ml, 42.0 mmol) and preL^A (2.06 g, 5.8 mmol) have been added, under vigorous stirring. In order to solubilize preL^A, the mixture has been heated to 65 °C. After that, the reaction mixture has been stirred at room temperature overnight. The solvent has been removed under reduced pressure. After addition of water (100 ml) and HCl 10% aqueous solution (10 ml), the formation of a yellow precipitate occurred. The solution has been extracted with CH_2Cl_2 (3x60 ml). The organic phase has been dried over $MgSO_4$ and the solvent has been removed under reduced pressure and the resulting yellow powder has been purified by recrystallization from ethyl acetate/n-hexane (1:2). The final product is obtained as yellow microcrystals (2.20 g). Yield: 70%.

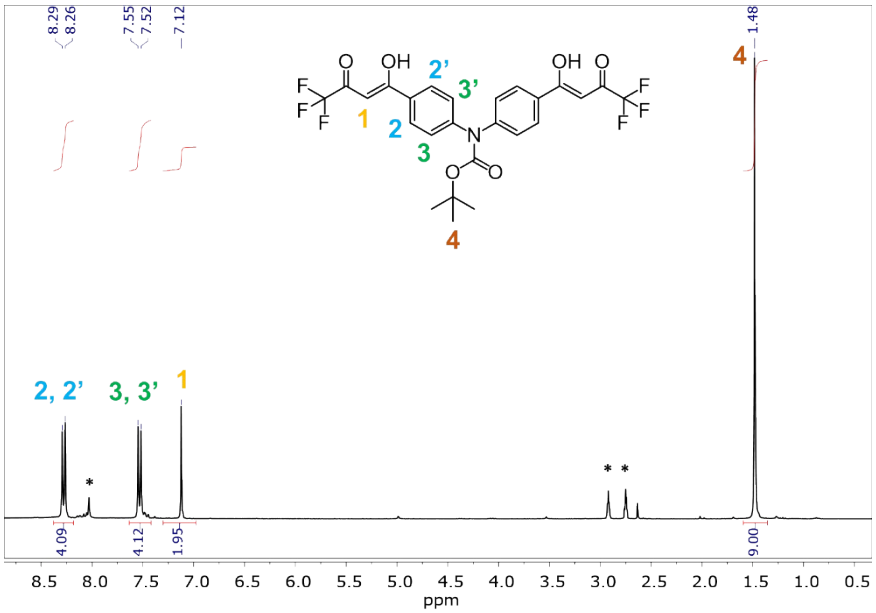

Fig. S1 ^{1}H-NMR spectra (25 °C, 300 MHz, DMF-d_7) of the ligand L^{A}

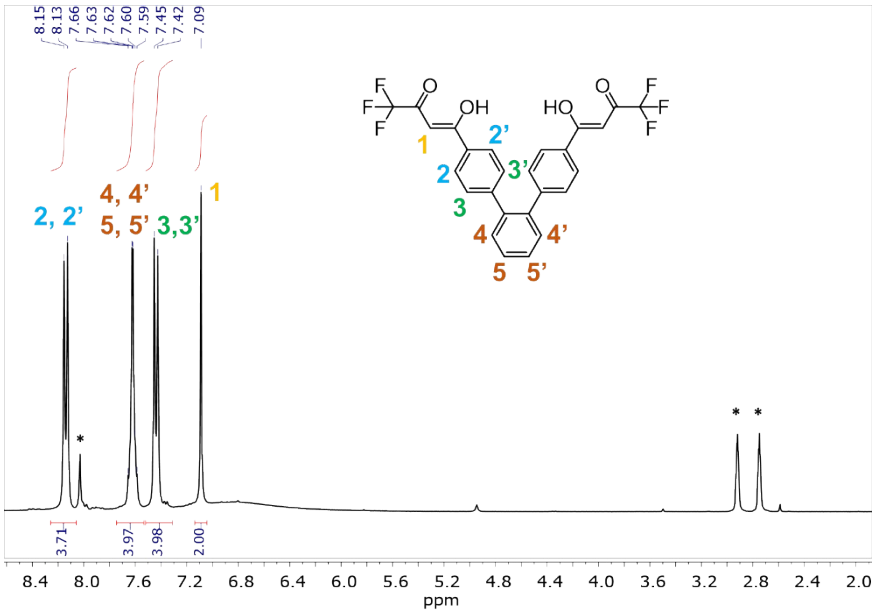

Fig. S2 ^{1}H-NMR spectra (25 °C, 300 MHz, DMF-d_7) of the ligand L^{B}

L^{B}: synthesized by a previous methodology.[2] Metallic Na (0.69 g, 30.0 mmol) has been dissolved in absolute ethanol (50 ml), in a 100 ml 3 necks round bottom flask, under argon atmosphere. After the solution reached room temperature, ethyl trifluoroacetate (5.0 ml, 42.0 mmol) and $preL^{B}$ (1.92 g, 6.1 mmol) have been added, under vigorous stirring. In order to solubilize $preL^{B}$, the mixture has been heated to 65 °C. After that, the reaction mixture has been stirred at room temperature overnight. The solvent has been removed under reduced pressure. After addition of water (100 ml) and HCl 10% aqueous solution (10 ml), the formation of a white precipitate occurred. The solution

has been extracted with CH_2Cl_2 (3x60 ml). The organic phase has been dried over $MgSO_4$ and the solvent has been removed under reduced pressure and the resulting yellow powder has been purified by recrystallization from acetonitrile at -18 °C. The final product is obtained as crystals (2.00 g). Yield: 64%.

L^M: synthesized by a previous methodology.[2] Metallic Na (0.70 g, 30.4 mmol) has been dissolved in absolute ethanol (50 ml), in a 100 ml 3 necks round bottom flask, under argon atmosphere. After the solution reached room temperature, ethyl trifluoroacetate (5.0 ml, 42.0 mmol) and $preL^M$ (1.57 g, 6.2 mmol) have been added, under vigorous stirring. In order to solubilize $preL^M$, the mixture has been heated to 65 °C. After that, the reaction mixture has been stirred at room temperature overnight. The solvent has been removed under reduced pressure. After addition of water (100 ml) and HCl 10% aqueous solution (10 ml), the formation of a pale-yellow precipitate occurred. The solution has been extracted with CH_2Cl_2 (3x60 ml). The organic phase has been dried over $MgSO_4$ and the solvent has been removed under reduced pressure and the resulting pale-yellow powder has been purified by recrystallization from acetonitrile at -18 °C. The final product is obtained as white crystals (1.74 g). Yield: 63%.

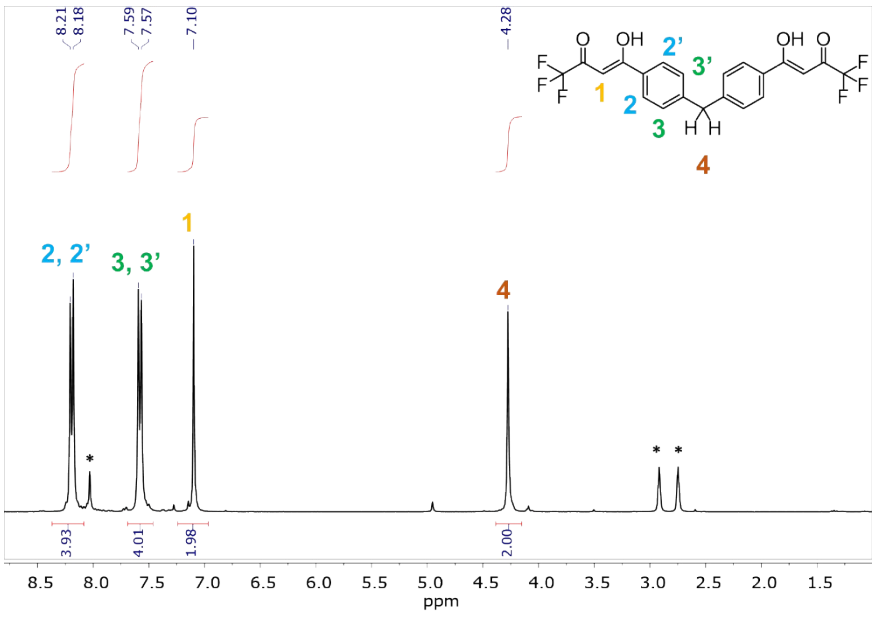

Fig. S3 ^{1}H-NMR spectra (25 °C, 300 MHz, DMF-d_7) of the ligand L^M

1.2. Cages synthesis

All the cages have been synthesized by a previous methodology.[2] For all the syntheses, the ratio La^{3+}:ligand:base used is equal to 1:2.5:5. All the $\{[La_2L^X_4](B)_2\}$ cages have been obtained with the following general procedure. The ligand (0.05 mmol) and the base (dicyclohexylamine, DCHA, 0.1 mmol) have been dissolved in 5 ml of ethanol. To this solution, a solution of $La(NO_3)_3{\cdot}6H_2O$ (0.020 mmol) in 2 ml of ethanol, has been added dropwise. The formation of a white precipitate occurred. The mixture has been left under vigorous stirring for 3 hours, then filtered and the obtained powder has been washed with cold ethanol to give the pure product. Yield of $\{[La_2L^A_4](DCHA)_2\}$, $\{[La_2L^B_4](DCHA)_2\}$ and $\{[La_2L^M_4](DCHA)_2\}$ respectively 57%, 72%, 71%.

$\{[La_2L^A_4](DCHA)_2\}$. ATR-FT-IR (cm^{-1}): 2937 (w), 2863 (w), 1607 (s), 1559 (m), 1527 (m), 1497 (m) 1460 (m), 1313 (m), 1286 (s), 1244 (m), 1179 (s), 1131 (m), 1064 (m), 1015 (w), 941 (w), 769 (m), 698(m). EA: calc. C 52.89 %, H 4.44 %, N 2.98 %; exp. C 52.95 %, H 4.54 %, N 2.86 %

$\{[La_2L^B_4](DCHA)_2\}$. ATR-FT-IR (cm^{-1}): 2946 (w), 2855 (w), 1609 (s), 1558 (m), 1527 (m), 1462 (m), 1312 (m), 1290 (s), 1243 (m), 1183 (s), 1134 (s), 1069 (w), 1007 (w), 938 (w), 792 (s), 762(s), 670 (s). EA: calc. C 57.80 %, H 3.94 %, N 1.05 %; exp. C 57.76 %, H 3.88 %, N 0.99 %

$\{[La_2L^M_4](DCHA)_2\}$. ATR-FT-IR (cm^{-1}): 2938 (w), 2855 (w), 1602 (s), 1562 (m), 1498 (m), 1463 (m), 1313 (m), 1283 (s), 1243 (m), 1179 (s), 1131 (s), 1067 (w), 1017 (w), 942 (w), 771 (m), 700(m). EA calc. C 53.79 %, H 4.01 %, N 1.16 %; exp. C 53.75 %, H 4.05 %, N 1.11 %

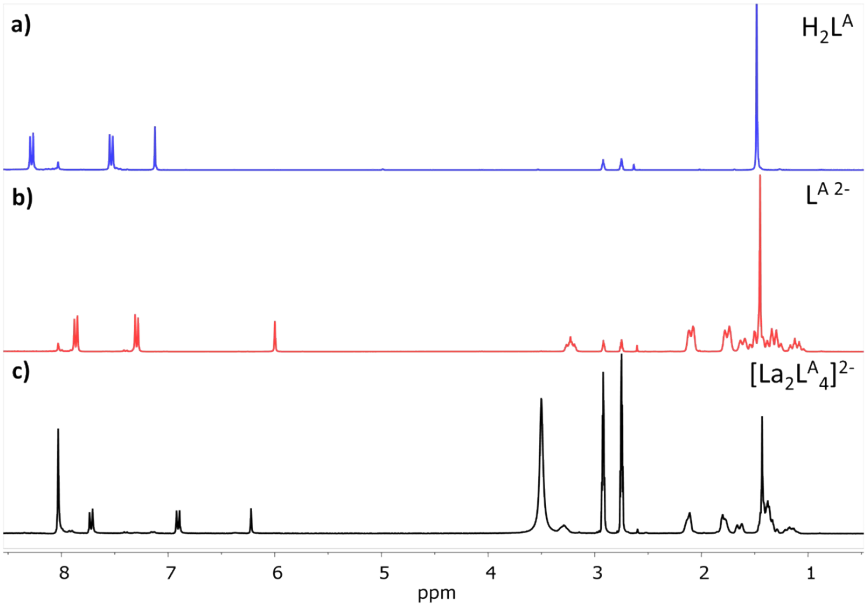

Fig. S4 ^{1}H-NMR spectra (25 °C, 300 MHz, DMF-d_7) of the ligand L^A a) protonated, b) deprotonated by DCHA and c) coordinated to La^{3+} (black).

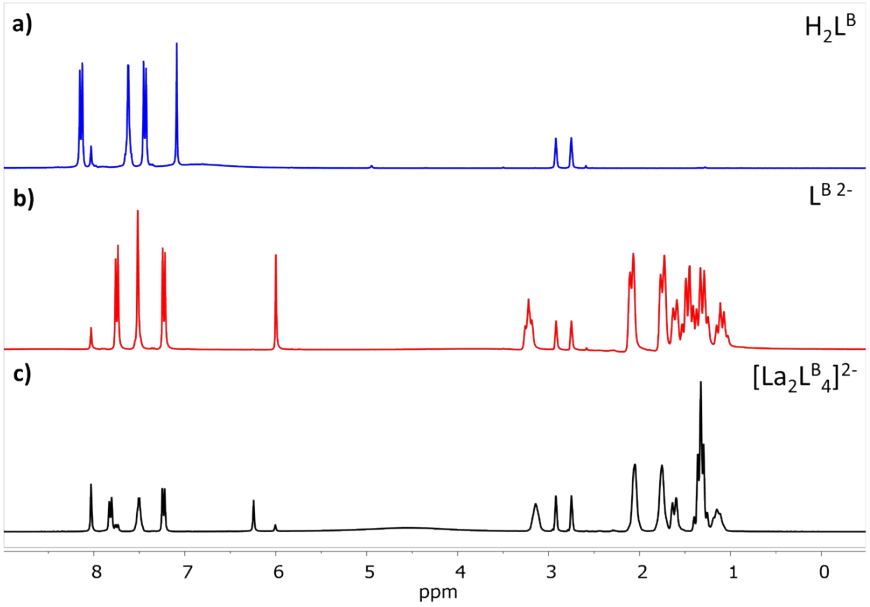

Fig. S5 ^{1}H-NMR spectra (25 °C, 300 MHz, DMF-d_7) of the ligand L^B a) protonated, b) deprotonated by DCHA and c) coordinated to La^{3+} (black).

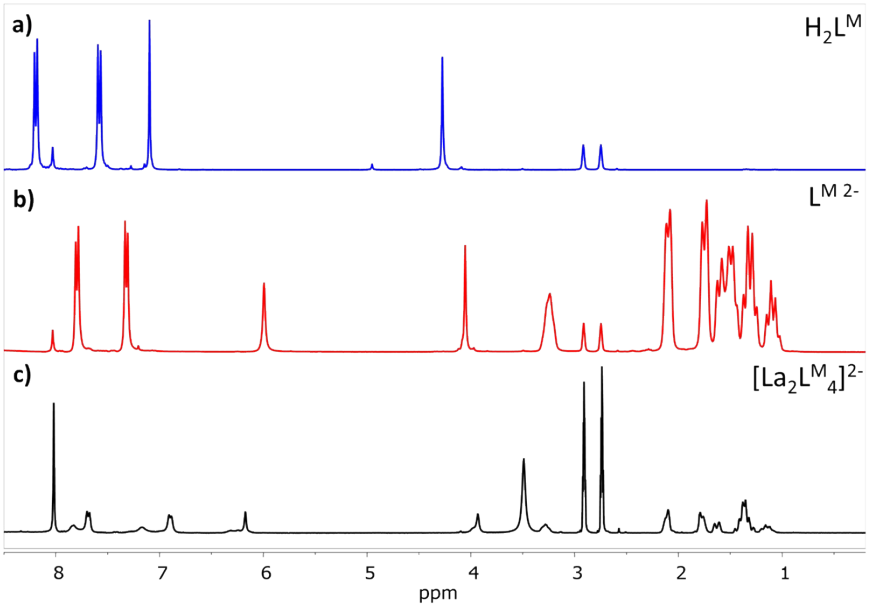

Fig. S6 ^{1}H-NMR spectra (25 °C, 300 MHz, DMF-d_7) of the ligand L^M a) protonated, b) deprotonated by DCHA and c) coordinated to La^{3+} (black).

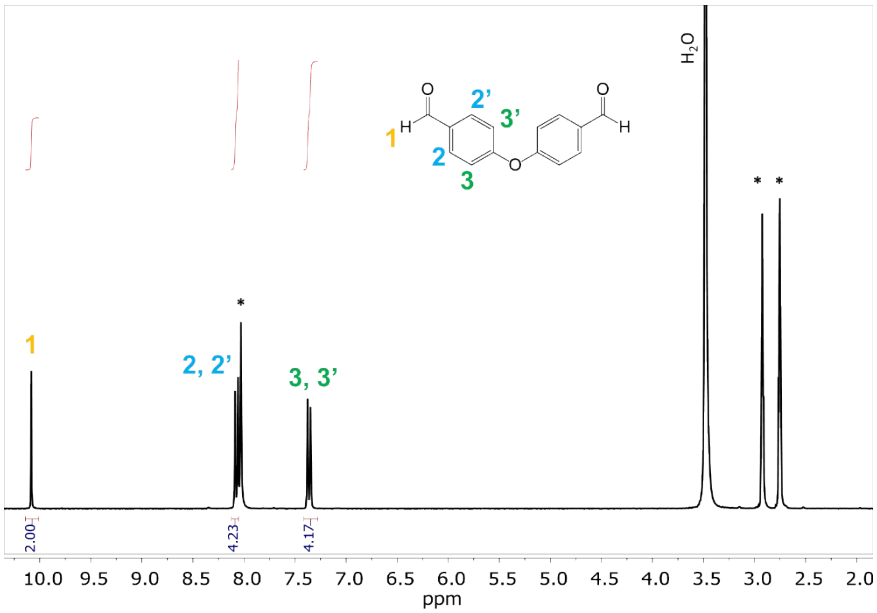

Fig. S7 ^{1}H-NMR spectra (25 °C, 300 MHz, DMF-d_7) of 4-(4-formylphenoxy)benzaldehyde used as imternal standard.

1.3. Diffusion coefficients

Table S1 Diffusion coefficient D and hydrodynamic radius r_H in DMF-d_7 for the species $[La_2L^A]^{4+}$, $[La_2L^A{}_2]^{2+}$, $[La_2L^A{}_3]$ and $[La_2L^A{}_4]^{2-}$.

Species	**$[La_2L^A]^{4+}$**	**$[La_2L^A{}_2]^{2+}$**	**$[La_2L^A{}_3]$**	**$[La_2L^A{}_4]^{2-}$**
Diffusion coefficient D (m^2/s)	$2.61\cdot10^{-10}$	$2.64\cdot10^{-10}$	$2.54\cdot10^{-10}$	$2.52\cdot10^{-10}$
Hydrodinamic radius r_H (Å)	10.7	10.6	11.0	11.1

2. Formation studies

The following solutions have been prepared: 2.8 mg of $La(NO_3)_3\cdot6H_2O$ (6.5 µmol) and 3.3 mg of 4-(4-formylphenoxy) benzaldehyde (14.6 µmol) in 2.25 mL of DMF-d_7; 17.5 mg of L^A (32.1 µmol) and 13 µL of DCHA (2.0 equivalents) in 0.750 mL of DMF-d_7; 16.8 mg of L^B (33.2 µmol) and 13 µL of DCHA (2.0 equivalents) in 0.750 mL of DMF-d_7; 14.4 mg of L^M (32.4 µmol) and 13 µL of DCHA (2.0 equivalents) in 0.750 mL of DMF-d_7. The $La(NO_3)_3\cdot6H_2O$ solution has been divided into three aliquotes of 0.730 µL. To each aliquote, different amounts of the three ligands solutions have been added. ^{1}H-NMR spectrum, for each different La:L^X ratio, was recorded immediately after the ligand addition and once the equilibrium was reached.

In a similar manner, ESI-MS spectra were collected in both positive and negative modes after the addition of 0.25, 0.5, 1.0, 1.5, 2.0, and 2.5 equivalents of deprotonated ligand L^A to a stock solution of $La(NO_3)_3\cdot6H_2O$ $1.0\cdot10^{-3}$ M in DMF diluted at $1.0\cdot10^{-6}$ M with CH_3CN immediately prior to record the spectra.

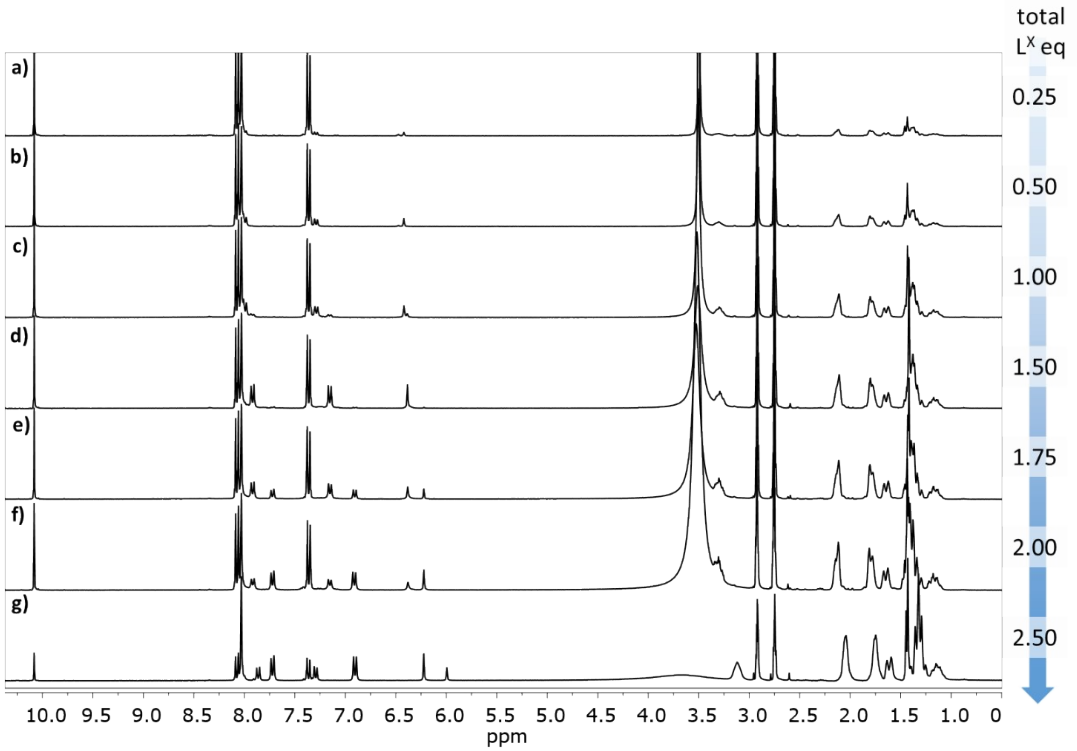

Fig. S8 ^{1}H-NMR spectra (25 °C, 300 MHz, DMF-d_7) of $[La_2L^{A}_{y}]^{n}$ with total added equivalents of ligand: a) 0.25 eq, b) 0.50 eq, c) 1.00 eq, d) 1.50 eq, e) 1.75 eq, f) 2.00 eq, and g) 2.50 eq.

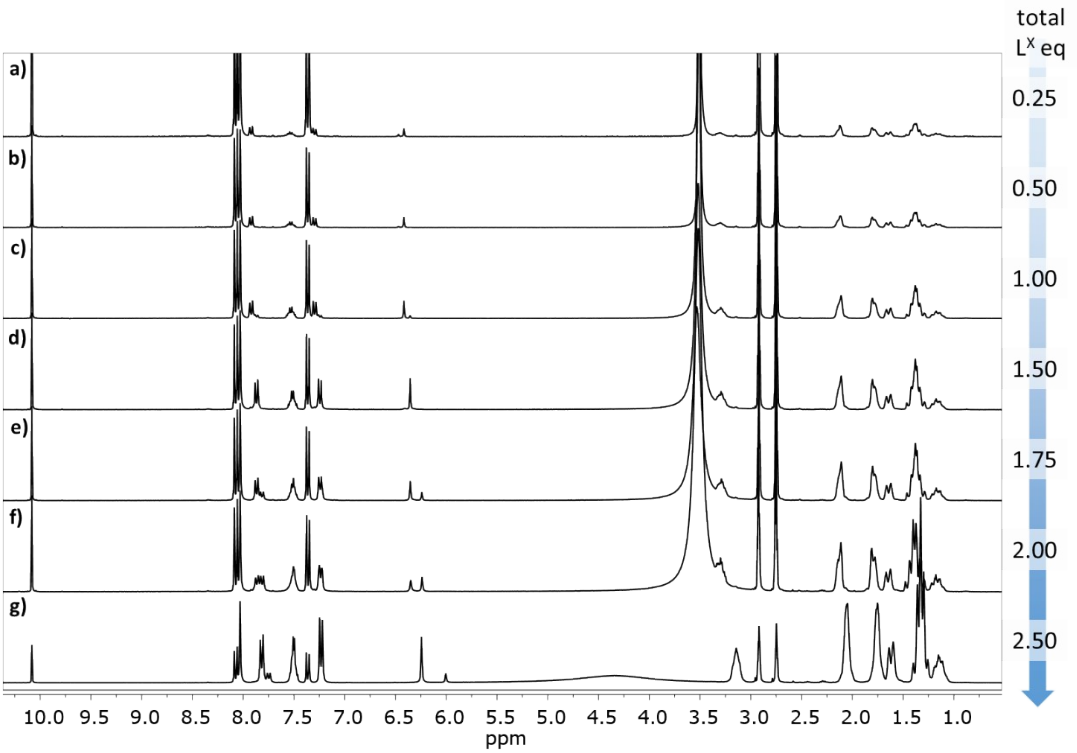

Fig. S9 ^{1}H-NMR spectra (25 °C, 300 MHz, DMF-d_7) of $[La_2L^{B}_{y}]^{n}$ with total added equivalents of ligand: a) 0.25 eq, b) 0.50 eq, c) 1.00 eq, d) 1.50 eq, e) 1.75 eq, f) 2.00 eq, and g) 2.50 eq.

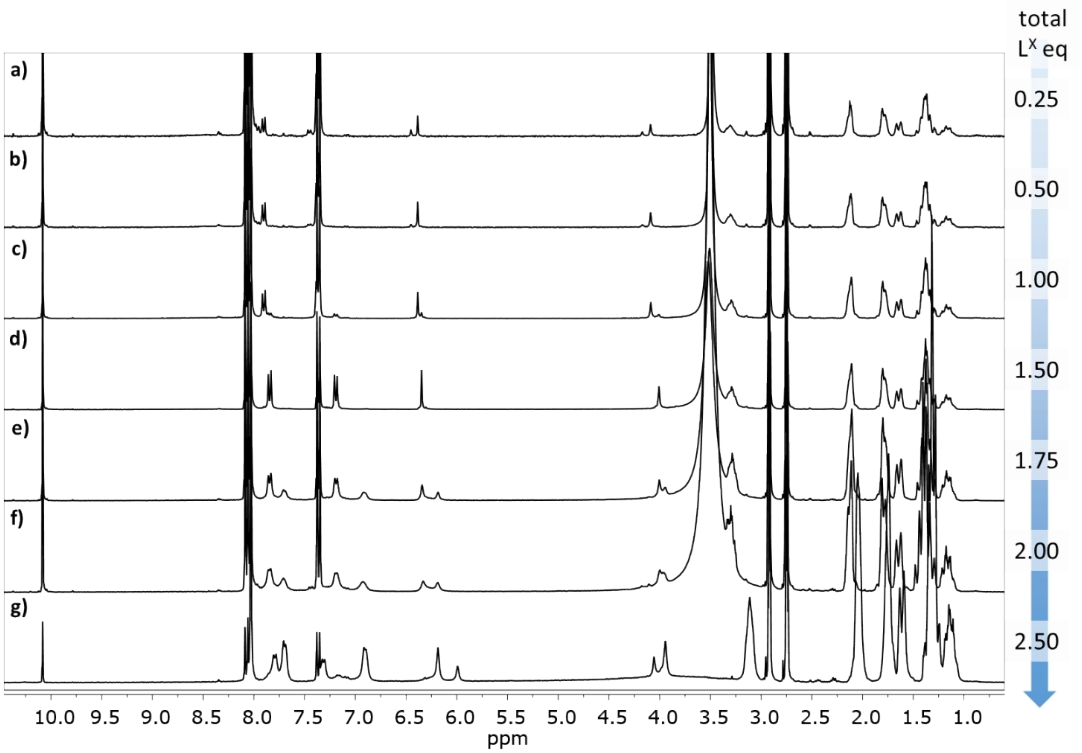

Fig. S10 ^{1}H-NMR spectra (25 °C, 300 MHz, DMF-d_7) of $[La_2L^M_y]^n$ with total added equivalents of ligand: a) 0.25 eq, b) 0.50 eq, c) 1.00 eq, d) 1.50 eq, e) 1.75 eq, f) 2.00 eq, and g) 2.50 eq.

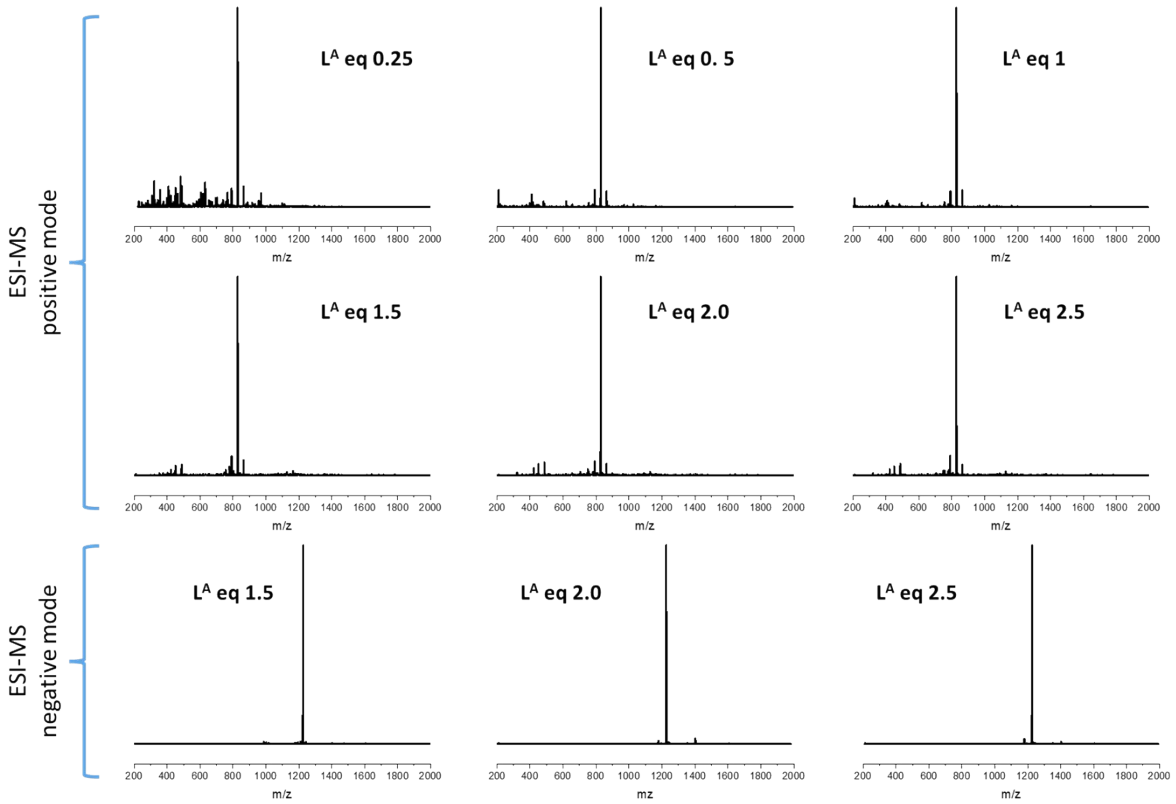

Fig. S11 ESI-MS spectra at different equivalents of L^A. Experimental and calculated isotopic patterns for the species centred at 828 m/z (positive mode) and the species centred at 1126 m/z (negative mode) are reported in Figure 1h and 1i of the main article.

Table S2 Total added L^A equivalents, the detected $[La_2L^A_y]^n$ species (where n = 4+, 2+, 0, 2- and y = 1, 2, 3, 4 respectively) through ^{1}H-NMR analyses and their relative amounts.

added L^A eq	$[La_2L^A_y]^n$ cages with different La:L^A ratio			
	2:1	2:2	2:3	2:4
0.25	$[La_2L^A]^{4+}$ (49%)	$[La_2L^A_2]^{2+}$ (51%)		
0.50	$[La_2L^A]^{4+}$ (32%)	$[La_2L^A_2]^{2+}$ (68%)		
1.00		$[La_2L^A_2]^{2+}$ (80%)	$[La_2L^A_3]$ (20%)	
1.50			$[La_2L^A_3]$ (100%)	
2.00			$[La_2L^A_3]$ (50%)	$[La_2L^A_4]^{2-}$ (50%)
2.50				$[La_2L^A_4]^{2-}$ (100%)

Table S3 Total added L^B equivalents, the detected $[La_2L^B_y]^n$ species (where n = 4+, 2+, 0, 2- and y = 1, 2, 3, 4 respectively) through ^{1}H-NMR analyses and their relative amounts.

added L^B eq	$[La_2L^B_y]^n$ cages with different La:L^B ratio			
	2:1	2:2	2:3	2:4
0.25	$[La_2L^B]^{4+}$ (34%)	$[La_2L^B_2]^{2+}$ (66%)		
0.50	$[La_2L^B]^{4+}$ (20%)	$[La_2L^B_2]^{2+}$ (80%)		
1.00		$[La_2L^B_2]^{2+}$ (88%)	$[La_2L^B_3]$ (12%)	
1.50			$[La_2L^B_3]$ (100%)	
2.00			$[La_2L^B_3]$ (56%)	$[La_2L^B_4]^{2-}$ (44%)
2.50				$[La_2L^B_4]^{2-}$ (100%)

Table S4 Total added L^M equivalents, the detected $[La_2L^M_y]^n$ species (where n = 4+, 2+, 0, 2- and y = 1, 2, 3, 4 respectively) through ^{1}H-NMR analyses and their relative amounts.

added L^M eq	$[La_2L^M_y]^n$ cages with different La:L^M ratio			
	2:1	2:2	2:3	2:4
0.25	$[La_2L^M]^{4+}$ (47%)	$[La_2L^M_2]^{2+}$ (53%)		
0.50	$[La_2L^M]^{4+}$ (26%)	$[La_2L^M_2]^{2+}$ (74%)		
1.00		$[La_2L^M_2]^{2+}$ (83%)	$[La_2L^M_3]$ (17%)	
1.50			$[La_2L^M_3]$ (100%)	
2.00			$[La_2L^M_3]$ (57%)	$[La_2L^M_4]^{2-}$ (43%)
2.50				$[La_2L^M_4]^{2-}$ (100%)

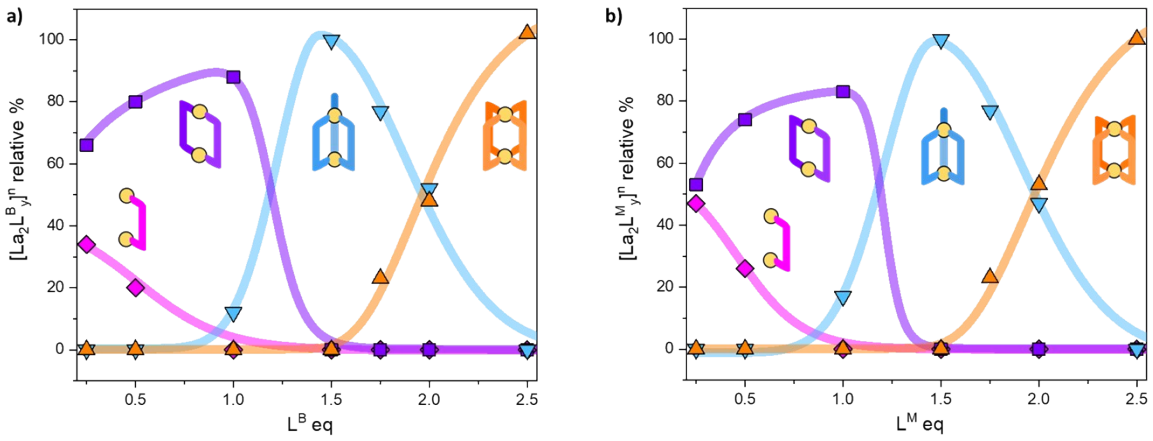

Fig. S12 Relative percentage of $[La_2L^B_y]^n$ and $[La_2L^M_y]^n$ species (where y = 1, 2, 3, 4 and n = 4+, 2+, 0, 2-, respectively) as derived through ^{1}H-NMR analyses following L^A ligand additions.

3. Determination of equilibrium constants

In presence of a slow equilibrium[3] between the species, the stepwise ($\mathbf{K_{2y}}$) and overall formation constants ($\boldsymbol{\beta_{2y}}$) can be obtained from ^{1}H-NMR spectra by integration of the peaks relative to the single species. Once obtained the relative concentration of the species, these values are converted into concentrations exploiting the internal standard (4-(4-formylphenoxy) benzaldehyde). The dialdehyde was chosen in order to have a stable standard, that does not react with the investigated systems, and whose NMR signals do not overlap with the cages ones. This assures the presence of easily integrable signals, which reduce the possible errors in the area integration and, hence, in the formation constants determination. Indeed, the concentrations of the different species in solution can be determined as follows:

$$n_{La_2L_y} = \frac{n_{st} * 2}{area_{st}} * \frac{area_{La_2L_y}}{x} \qquad eq.\ S1$$

$$\left[La_2L_y^n\right] = \frac{n_{La_2L_y}}{V_{tot}} \qquad eq.\ S2$$

$$\left[L^{2-}\right]_{tot} = \left[L^{2-}\right]^\circ = \left[L^{2-}\right]_{eq} + \sum_y y * \left[La_2L_y^n\right]_{eq} \qquad eq.\ S3$$

$$\left[La^{3+}\right]_{tot} = \left[La^{3+}\right]^\circ = \left[La^{3+}\right]_{eq} + \sum_y 2 * \left[La_2L_y^n\right]_{eq} \qquad eq.\ S4$$

Where $n_{La_2L_y}$is the number of moles of $[La_2L^X_y]^n$ species, n_{st} is the number of moles of the standard, $area_{La_2L_y}$ is the area of the α-proton (H_1) peak for the $[La_2L^X_y]^n$ system, $area_{st}$ is the area of the aldehyde proton (R-CHO) singlet of the standard, *y* is the number of coordinated ligands and the values in square brackets are initial (°) or equilibrium (eq) concentrations of species.

The signals of the different species are narrow and easily integrable. Nevertheless, for some pair of species, the α-proton singlets are partially overlapped, making the use of peaks deconvolution program necessary to opportunely calculate the peaks areas. In Fig. S12, an example of peaks deconvolution for the species $[La_2L^X_2]^{2+}$ and $[La_2L^X_3]$ is shown.

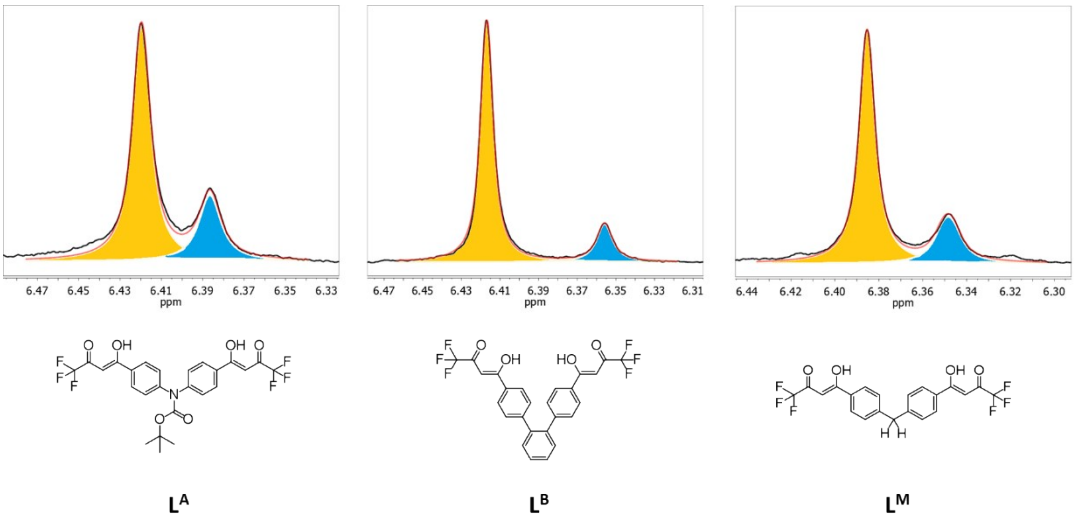

Fig. S13 ^{1}H-NMR spectra (25 °C, 300 MHz, DMF-d_7) in the α-proton region of $[La_2L^A_4]^{2-}$ (left), $[La_2L^B_4]^{2-}$ (center) and $[La_2L^M_4]^{2-}$ (right) after the addition of 1.00 eq of ligand. The deconvoluted peaks are shown in orange, $[La_2L^X_2]^{2+}$, and blue, $[La_2L^X_3]$; the sum is shown in red.

4. ^{1}H-NMR spectra at variable temperature

The following solutions have been prepared: 4.2 mg of $La(NO_3)_3{\cdot}6H_2O$ (9.7 µmol) in 2.0 mL DMF-d_7; 2.2 mg of 4-(4-formylphenoxy) benzaldehyde (9.9 µmol) in 0.140 mL of DMF-d_7; 8.4 mg of L^A (15.4 µmol) and 6.1 µL of DCHA (2.0 equivalents) in 0.200 mL of DMF-d_7; 7.8 mg of L^B (15.5 µmol) and 6.2 µL of DCHA (2.0 equivalents) in 0.200 mL of DMF-d_7; 7.3 mg of L^M (16.4 µmol) and 6.5 µL of DCHA (2.5 equivalents) in 0.200 mL of DMF-d_7. The $La(NO_3)_3{\cdot}6H_2O$ solution has been divided into three aliquots of 0.570 µL. To each aliquot, 19.5 µL of the benzaldehyde (13.8 µmol) and 2 equivalents of L^X has been added, respectively 72.0 µL, 71.0 µL and 67.0 µL for L^A, L^B and L^M.

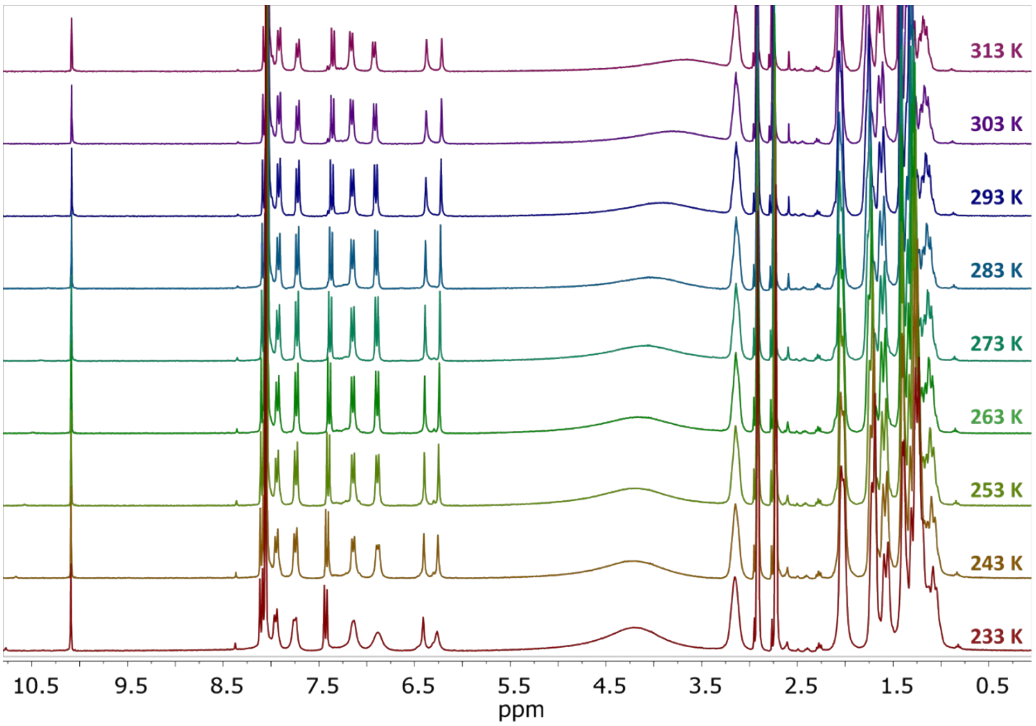

Fig. S14 ^{1}H-NMR spectra (25 °C, 300 MHz, DMF-d_7) of $[La_2L^{A}_{y}]^{n}$ with 2.00 total added equivalents of ligand in the range of temperature between 313 K and 233 K.

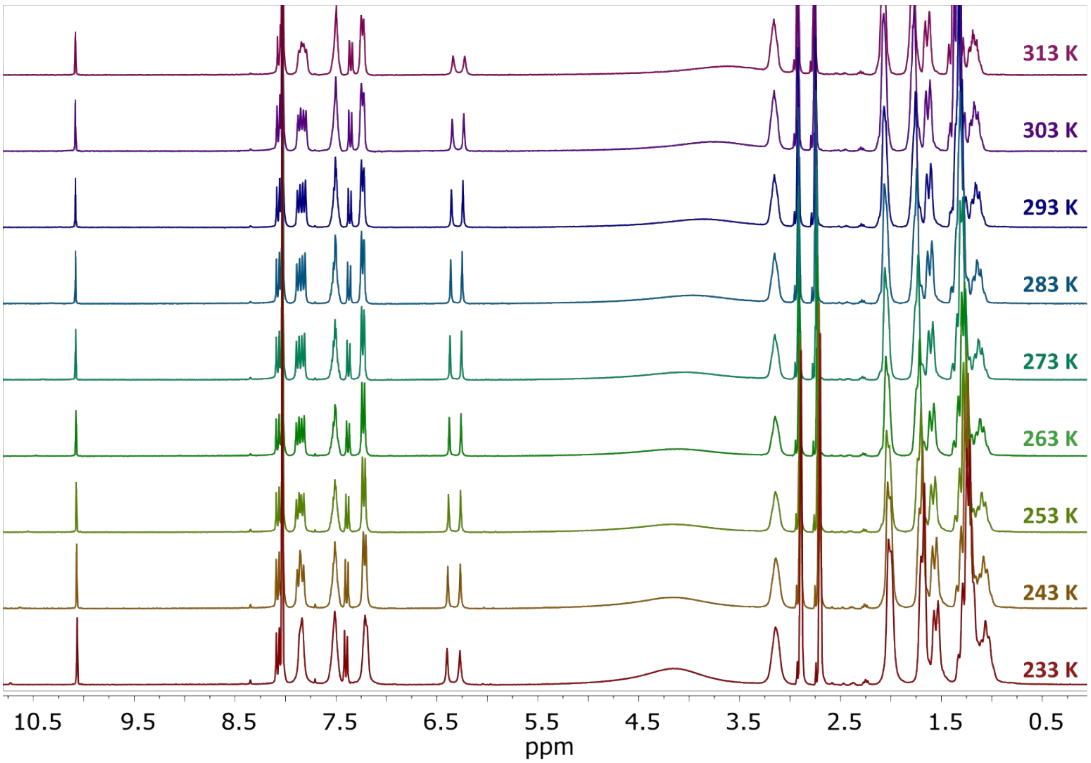

Fig. S15 ^{1}H-NMR spectra (25 °C, 300 MHz, DMF-d_7) of $[La_2L^{B}_{y}]^{n}$ with 2.00 total added equivalents of ligand in the range of temperature between 313 K and 233 K.

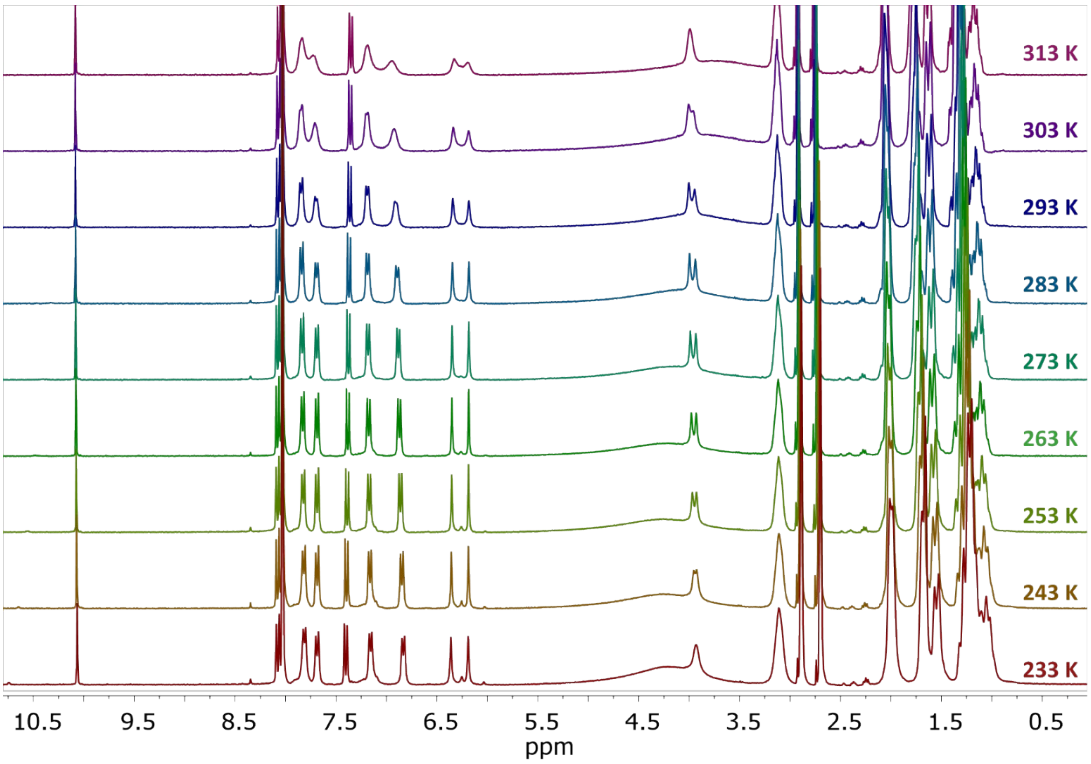

Fig. S16 ^{1}H-NMR spectra (25 °C, 300 MHz, DMF-d_7) of $[La_2L^M_y]^n$ with 2.00 total added equivalents of ligand in the range of temperature between 313 K and 233 K.

5. Van't Hoff plot

The van't Hoff plot is a graphical representation of the natural logarithm of the equilibrium constant (ln K) versus the reciprocal of the temperature (1/T) for a chemical reaction. Mathematically, the equation of the van't Hoff plot is:

$$\ln K\left(\frac{1}{T}\right) = -\frac{\Delta H}{k_b} * \frac{1}{T} + \frac{\Delta S}{k_b} \qquad eq.\ S5$$

Where ΔH is the enthalpy change of the reaction, ΔS is the entropy change of the reaction, k_b is the Boltzmann constant, and T is the temperature. Exploiting the expanded van't Hoff model,[4] than eq. S5 can be written as:

$$\ln K\left(\frac{1}{T}\right) = a + \frac{b}{T} + \frac{c}{T^2} \qquad eq.\ S6$$

Where a, b and c are parameters which are determined during the fitting process of lnK versus 1/T. Accordingly, ΔG(T), ΔH(T) and ΔS(T) can be written as:

$$\Delta G(T) = \Delta H - T\Delta S \qquad eq.\ S7$$

$$\Delta H(T) = -k_B\left(b + \frac{2c}{T}\right) \qquad eq.\ S8$$

$$\Delta S(T) = k_B\left(a - \frac{c}{T^2}\right) \qquad eq.\ S9$$

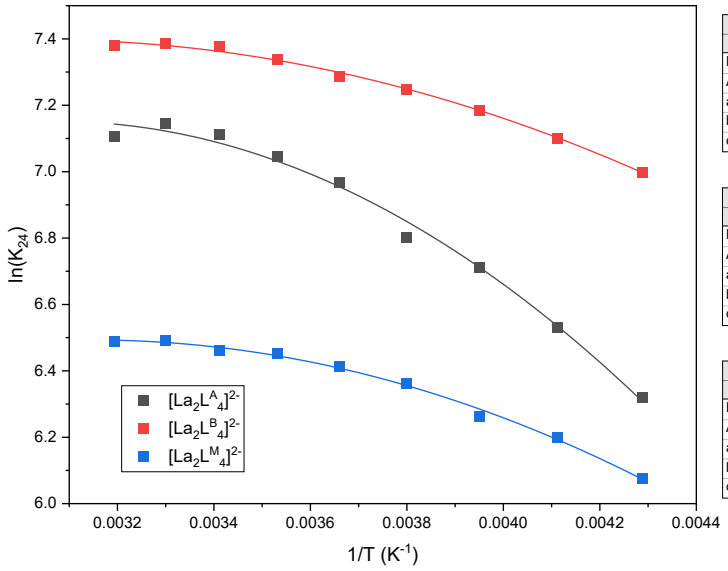

a + b * x + c * (x ^ 2)	[LaLA4]2-
Reduced Chi-S	8.97182E-4
Adj. R-Square	0.98943
a	1.75468 ± 1.26021
b	3512.51841 ± 679.52791
c	-571504.96998 ± 90934.1

a + b * x + c * (x ^ 2)	[LaLB4]2-
Reduced Chi-S	9.08058E-5
Adj. R-Square	0.99516
a	5.02344 ± 0.40092
b	1562.16591 ± 216.1842
c	-256963.23047 ± 28929.6

a + b * x + c * (x ^ 2)	[LaLM4]2-
Reduced Chi-S	1.29368E-4
Adj. R-Square	0.99398
a	3.30569 ± 0.47854
b	2025.96068 ± 258.03617
c	-321938.27075 ± 34530.2

Fig. S17 Fitting of the experimental lnK with the expanded van't Hoff model (eq. S6).

6. Computational details

Structure optimization. The Amsterdam Density Functional (ADF) program (version 2013.01) was employed for all optimized structure calculations.[5] The generalized gradient approximation (GGA) PBE ex-change-correlation functional[6] was used, combined with the TZ2P basis set. The TZ2P is a Slater-type triple-ζ quality basis set augmented with two sets of polarization functions for all the atoms. The choice of PBE functional is due to the preview literature on similar systems.[1,7,8] Scalar relativistic effects were considered using the scalar zeroth-order regular approximation (ZORA).[9] The numerical integration grid is a refined version of the fuzzy-cells integration scheme developed by Becke. Solvent effects were also considered using the COnductor-like Screening MOdel (COSMO)[10] with the default parameters for acetonitrile (dielectric constant ε = 37.5 and a solvent-

excluding surface radius of 2.76 Å). The solvent used in the experimental study is the DMF, but it is not present in the ADF COSMO model. Then, the acetonitrile is chosen because it has similar dielectric constant parameter to DMF. Calculations with the dispersion correction correctly reproduce the geometrical structure for $[La_2L_4]^{2-}$ cages, but for the other cages with a lower number of coordinated ligands, the ligands tend to form unreliable close contacts with each other. This is probably due to the absence of explicit solvent molecules between the ligands that mitigate the dispersion interactions. In the $[La_2L_4]^{2-}$ cages, the steric hindrance probably prevents this behaviour. For this reason, all calculations for $[La_2L^A_y(DMF)_{16-4y}]^n$ species (where y = 1, 2, 3, 4 and n = 4+, 2+, 0, 2-, respectively) were performed without the inclusion of the dispersion corrections. On the contrary, for the smaller models $[La_2L_y(DMF)_{16-4y}]^n$ used for the calculations of the thermochemistry parameters, the dispersion corrections were included because no unreliable close contacts were observed between the ligands. Dispersion corrections were included as implemented by Grimme[11] (Grimme3 BJDAMP) model. Solvent effects and dispersion corrections were included by reoptimizing the structure.

Thermochemistry calculations. Thermochemistry parameters (the enthalpy H, the entropy S and the Gibbs free energy G) were also calculated by using the Amsterdam Density Functional (ADF) program (version 2013.01) on optimized structures of the $[La_2L_y(DMF)_{16-4y}]^n$ species with the same level of theory used for the optimization calculations. The Keyword THERMO is adopted where T_{min} is 233 K and T_{max} is 313 K with nT=10, where nT is the number of steps by which the temperature interval is scanned.

The Gibbs free energy is given by the standard thermodynamic definition:

$$G = H - T \cdot S \qquad eq.S10$$

where H is the enthalpy, S is the entropy, and T is the temperature. For the enthalpy H:

$$H = U + pV = E_{el} + E_{nie} + pV \qquad eq.\ S11$$

$$E_{nie} = ZPE + \ 3k_BT + small\ correction\ term \qquad eq.\ S12$$

where U is the internal energy which can be decomposed into E_{el}, the total electronic energy and E_{nie}, the nuclear internal energy. In the E_{nie}, ZPE is the zero-temperature vibrational energy (*i.e.* the Zero Point Energy) and 3 k_BT = 3/2 k_BT for rotation, 3/2 k_BT for translation (1/2 for each degree of

freedom). The small correction term is a term due to the vibration partition function, depending on the temperature.

The thermodynamic parameters (enthalpies, entropies, and Gibbs free energies) were calculated for each species involved in the flowing equilibria.

$$La(DMF)_8^{3+} + acac^- \rightleftharpoons La(acac)(DMF)_6^{2+} + 2\,DMF \qquad eq.\,13$$

$$La(acac)(DMF)_6^{2+} + acac^- \rightleftharpoons La(acac)_2(DMF)_4^{+} + 2\,DMF \qquad eq.\,14$$

$$La(acac)_2(DMF)_4^{+} + acac^- \rightleftharpoons La(acac)_3(DMF)_2 + 2\,DMF \qquad eq.15$$

$$La(acac)_3(DMF)_2 + acac^- \rightleftharpoons La(acac)_4^- + 2\,DMF \qquad eq.\,16$$

To calculate the ΔG, ΔH and TΔS values associated with a particular reaction, the values for the reactant and product molecules must be added (products) or subtracted (reagents) for each molecule, in proportion to the number of molecules involved in the reaction.

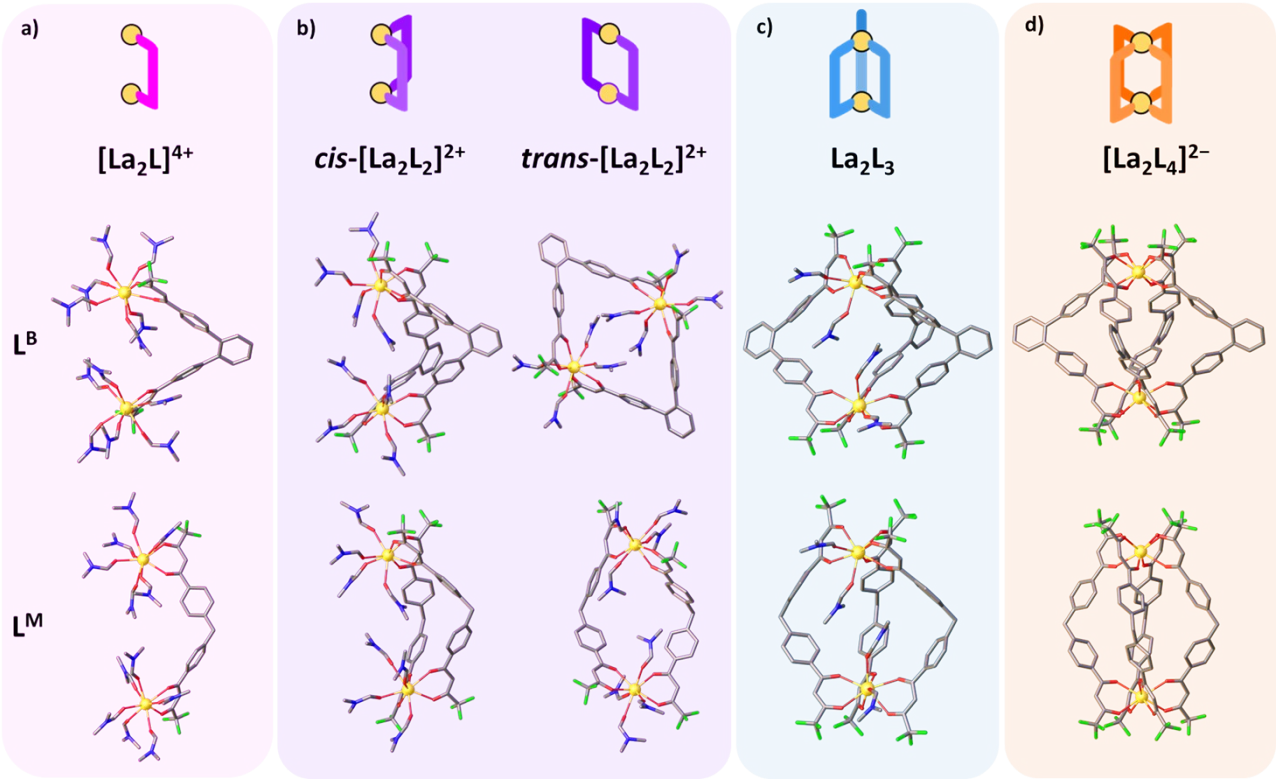

Fig. S18 DFT optimized structures for DMF solvated $[La_2L^A_y(DMF)_{16-4y}]^n$ species (where y = 1, 2, 3, and 4 and n = 4+, 2+, 0, and 2−, respectively). a) $[La_2L^A(DMF)_{12}]^{4+}$, b) *cis*-$[La_2L^A_2(DMF)_8]^{2+}$ and *trans*-$[La_2L^A_2(DMF)_8]^{2+}$, c) $[La_2L^A_3(DMF)_4]$, d) $[La_2L_4]^{2-}$. Red, blue, grey and green sticks represent O, N, C, and F atoms, respectively. The yellow spheres are La atoms. H atoms are omitted for clarity.

7. References

1 M. Rancan, M. Rando, L. Bosi, A. Carlotto, R. Seraglia, J. Tessarolo, S. Carlotto, G. H. Clever and L. Armelao, *Inorg Chem Front*, 2022, **9**, 4495–4505.

2 M. Rancan, J. Tessarolo, A. Carlotto, S. Carlotto, M. Rando, L. Barchi, E. Bolognesi, R. Seraglia, G. Bottaro, M. Casarin, G. H. Clever and L. Armelao, *Cell Rep Phys Sci*, 2022, **3**, 100692.

3 I. R. Kleckner and M. P. Foster, *Biochimica et Biophysica Acta (BBA) - Proteins and Proteomics*, 2011, **1814**, 942–968.

4 C. G. Maier and K. K. Kelley, *J Am Chem Soc*, 1932, **54**, 3243–3246.

5 G. te Velde, F. M. Bickelhaupt, E. J. Baerends, C. Fonseca Guerra, S. J. A. van Gisbergen, J. G. Snijders and T. Ziegler, *J Comput Chem*, 2001, **22**, 931–967.

6 J. P. Perdew, K. Burke and M. Ernzerhof, *Phys Rev Lett*, 1996, **77**, 3865.

7 Y. Zhou, Y. Yao, Z. Cheng, T. Gao, H. Li and P. Yan, *Inorg Chem*, 2020, **59**, 12850–12857.

8 S. Carlotto, L. Armelao and M. Rancan, *Int J Mol Sci*, 2022, **23**, 10619.

9 E. van Lenthe, A. Ehlers and E.-J. Baerends, *J Chem Phys*, 1999, **110**, 8943–8953.

10 C. C. Pye, T. Ziegler, E. Van Lenthe and J. N. Louwen, *Can J Chem*, 2009, **87**, 790–797.

11 S. Grimme, S. Ehrlich and L. Goerigk, *J Comput Chem*, 2011, **32**, 1456–1465.